Article

Magma Mixing Genesis of the Mafic Enclaves in the Qingshanbao Complex of Longshou Mountain, China: Evidence from Petrology, Geochemistry, and Zircon Chronology

Wenheng Liu [1,2,3,*], Xiaodong Liu [4], Jiayong Pan [1], Kaixing Wang [5], Gang Wang [6], Yuben Niu [5] and Wanjing Gong [5]

1   State Key Laboratory of Nuclear Resources and Environment, East China University of Technology, Nanchang 330013, China; jypan@ecit.cn

2   Center of Geological Resource Economics and Management Research, East China University of Technology, Nanchang 330030, China

3   Key Laboratory for Digital Land and Resources of Jiangxi Province, East China University of Technology, Nanchang 330030, China

4   Jiujiang University, Jiujiang 332000, China; xdliu@ecit.cn

5   School of Earth Sciences, East China University of Technology, Nanchang 330030, China; xy2gmo02@ecit.cn (K.W.); benniu2220@sina.com (Y.N.); jelly6042@163.com (W.G.)

6   Research Institute No. 203 of Nuclear Industry, Xianyang 712000, China; wgang515@163.com

*   Correspondence: liuwh@ecit.cn; Tel.: +86-0791-8389-7218

check for updates

Abstract: The Qingshanbao complex, part of the uranium metallogenic belt of the Longshou-Qilian mountains, is located in the center of the Longshou Mountain next to the Jiling complex that hosts a number of U deposits. However, little research has been conducted in this area. In order to investigate the origin and formation of mafic enclaves observed in the Qingshanbao body and the implications for magmatic-tectonic dynamics, we systematically studied the mineralogy, petrography, and geochemistry of these enclaves. Our results showed that the enclaves contain plagioclase enwrapped by early dark minerals. These enclaves also showed round quartz crystals and acicular apatite in association with the plagioclase. Electron probe analyses showed that the plagioclase in the host rocks (such as K-feldspar granite, adamellite, granodiorite, etc.) show normal zoning, while the plagioclase in the mafic enclaves has a discontinuous rim composition and shows instances of reverse zoning. Major elemental geochemistry revealed that the mafic enclaves belong to the calc-alkaline rocks that are rich in titanium, iron, aluminum, and depleted in silica, while the host rocks are calc-alkaline to alkaline rocks with enrichment in silica. On Harker diagrams, SiO_2 contents are negatively correlated with all major oxides but K_2O. Both the mafic enclaves and host rock are rich in large ion lithophile elements such as Rb and K, as well as elements such as La, Nd, and Sm, and relatively poor in high field strength elements such as Nb, Ta, P, Ti, and U. Element ratios of Nb/La, Rb/Sr, and Nb/Ta indicate that the mafic enclaves were formed by the mixing of mafic and felsic magma. In terms of rare earth elements, both the mafic enclaves and the host rock show right-inclined trends with similar weak to medium degrees of negative Eu anomaly and with no obvious Ce anomaly. Zircon LA-ICP-MS (Laser ablation inductively coupled plasma mass spectrometry) U-Pb concordant ages of the mafic enclaves and host rock were determined to be 431.8 ± 5.2 Ma (MSWD (mean standard weighted deviation) = 1.5, *n* = 14) and 432.8 ± 4.2 Ma (MSWD = 1.7, *n* = 16), respectively, consistent with that for the zircon U-Pb ages of the granite and medium-coarse grained K-feldspar granites of the Qingshanbao complex. The estimated ages coincide with the timing of the late Caledonian collision of the Alashan Block. This comprehensive analysis allowed us to conclude that the mafic enclaves in the Qingshanbao complex were formed by the mixing of crust-mantle magma with mantle-derived magma due to underplating, which caused

partial melting of the ancient basement crust during the collisional orogenesis between the Alashan Block and Qilian rock mass in the early Silurian Period.

1. Introduction

Magma mixing is one of the important mechanisms for the formation of intermediate-acid intrusive rocks [1,2]. The study of magma mixing is important for understanding the crustal growth and evolution [3,4], crust-mantle interaction [5], magma dynamics [6], and mineralization of correlative metal deposits [7]. The mafic microgranular enclaves (MMEs) in the intermediate-acid intrusive rocks are important petrological indicators of magma mixing because of their special mineralogical and petrographic characteristics compared with their host rocks, and they are very good objects for studying the genesis of the intermediate-acid intrusive rocks and the geodynamic background of magmatism [8]. The Longshou Mountain uranium metallogenic belt, located on the southwestern margin of the North China Craton, had intensive magmatic activities during the Early Paleozoic, producing a large number of granite intrusions and sodium-metasomatic type uranium deposits [9]. The ore body is present in the sodium-metasomatic altered granite and is closely related to the magmatic rock and the post-magmatic alkaline hydrothermal fluid [10]. The Qingshanbao granite complex is located in the middle of the Longshou Mountain uranium metallogenic belt and contains secondary leaching-type uranium mineralization, whose primary ore should be sodium-metasomatic type uranium ore [11]. It has been found in the field that the dark-colored mafic microgranular enclaves in the Qingshanbao granite complex are intensively developed, but studies on the emplacement age, rock genesis, and tectonic setting are still insufficient. This paper aims to conduct detailed petrographic, mineralogical, geochemical, and zircon U-Pb geochronology studies on the Qingshanbao granite complex and its mafic microgranular enclaves, for a better understanding of the magma mixing genesis and magmatism tectonic setting. This study provides important evidence for the magma-mineralization of the Longshou Mountain uranium metallogenic belt.

2. Geological Summary

The Qingshanbao complex is located in the middle of the Longshou Mountain, ~2 km to the northeast of Hexibao town, in the Gansu Province, and to the south of the Jinchuan super-large Cu-Ni sulfide mining area. The Longshou Mountain research area is located on the southwestern margin of the Alashan uplift belt (Figure 1A,B). The earliest rocks in the area are the migmatite, interbedded with amphibolite and granitic gneiss of the Paleoproterozoic Longshou Mountain group, which are sourced from the metamorphic crystalline basement [10]. It is unconformably overlain by the Meso-Proterozoic Dunzigou Group and the Neoproterozoic Hanmushan Group. The Phanerozoic strata are scattered, the early Paleozoic strata are partially missing, and the Mesozoic-Cenozoic erathem is distributed in narrow fault basins in the mountains. Intrusive rocks found in this area include the ultramafic intrusive rocks that produce super-large Cu-Ni deposits and widely distributed granitoid. The folds and faults in the area are mainly northwest-trending and were probably formed by the tectonic movement of the early Paleozoic Northern Qilian fold system [9]. These structures control the distribution of strata and intrusive rocks in the area. Several anomalies in the background level of radiation associated with uranium, thorium, and potassium are observed in the area [10], as well as various types of uranium deposits and ore occurrences.
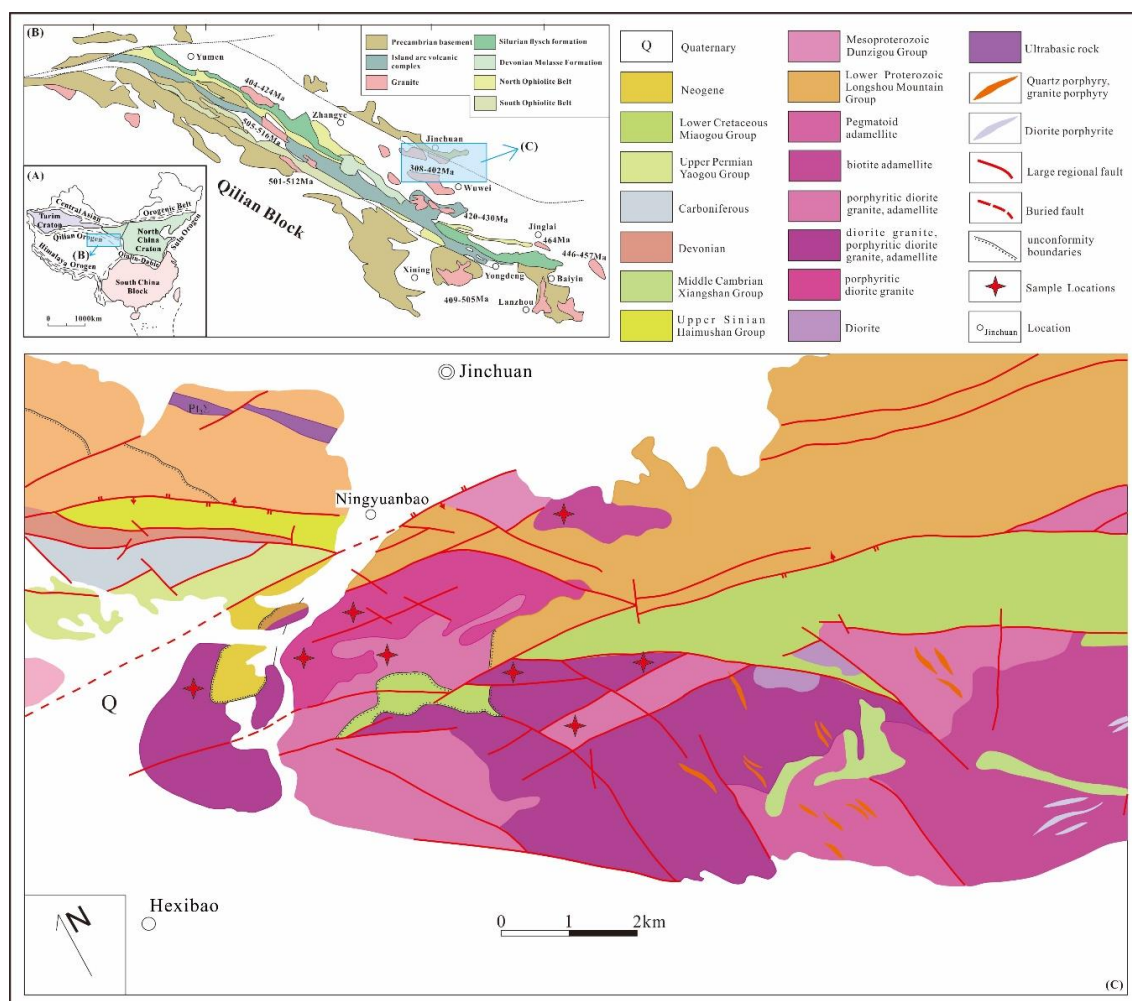
Figure 1. (**A**,**B**) Regional tectonic map of the Alashan uplift belt (based on Song et al. [12]). (**C**) Geological map of the Qingshanbao complex in the Longshou Mountain.

The exposed Qingshanbao complex is mainly composed of granitoids, including medium-coarse grained K-feldspar granite, adamellite, granodiorite, medium-coarse grained porphyraceous biotite granite, and fine-grained granite. Most of these igneous bodies intruded into the pre-Changcheng System Longshou Mountain Group, the Sinian Hanmu Mountain Group and the Cambrian Dahuang Mountain Group, and the exposed area is approximately 90 km^2 (Figure 1C). The mafic enclaves are widely distributed, mainly in the K-feldspar granite, adamellite and granodiorite.

3. Petrographic Characteristics

The mafic enclaves in the Qingshanbao complex have a darker color and finer grain size than the host rock. Most have rounded, water-drop, lenticular or elliptical shapes, with a diameter of 10–35 cm (Figure 2). While some mafic enclaves have clear boundaries with the host complex, others are elongated and the margins of the enclave are relatively diffuse, showing a gradual transition with the host. This observation indicates that the mafic enclaves and the host rock coexisted as fluids. Microscopically, the mafic enclaves generally have an idiomorphic or hypidiomorphic granular and massive texture. The mineral composition mainly includes plagioclase (40–50% in volume), hornblende (15–20%), biotite (25–35%) and quartz (10–15%), with typical structural features of magmatic rock. Compared with the felsic host rock, the contents of quartz in the mafic enclaves is significantly lower, while those of plagioclase and hornblende are significantly higher.

Figure 2. (**A**,**B**) Field occurrence of the mafic enclaves in the Qingshanbao complex of the Longshou Mountain.

The Plagioclase crystals in the mafic enclaves occasionally show complex zoning (Figure 3B,C), which may be related to the incorporation of mafic-intermediate material during growth. In addition, some of the plagioclase crystals contain dark minerals and rounded quartz (Figure 3D,E). The distribution of apatite in the host rock and in the mafic enclaves is extensive (Figure 3F). Apatite in the host rock is generally short and prismatic with an aspect ratio of approximately 3–4, while those in the mafic enclaves are generally fine and acicular, approximately 0.05–0.15 mm in length and 0.01 mm in width, with an aspect ratio ranging between 5 and 15.
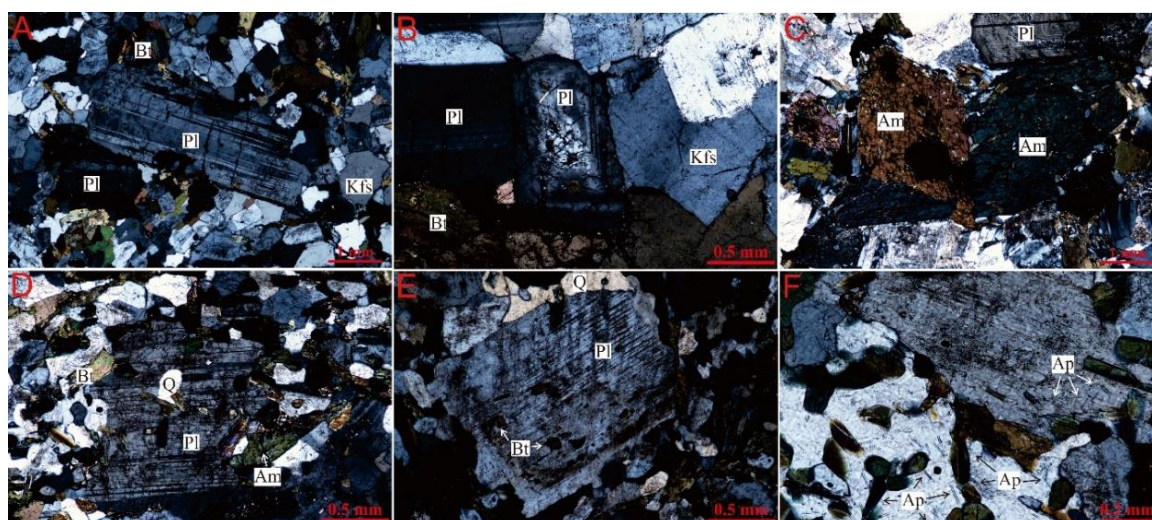

Figure 3. Photo-micrographs showing the mineralogy and textures of the mafic enclaves. (**A**) Euhedral tabular plagioclase in the dark color pack with hypautomorphic granular potassium feldspar and biotite. (**B**) Complex zoning in a plagioclase crystal. (**C**) Highly rhombohedral hornblende crystal and zoned plagioclase crystal. (**D**) Plagioclase enwrapped by rounded quartz. (**E**) Biotite inclusion in a plagioclase crystal that shows a dissolution texture and a scalloped edge. (**F**) Elongated acicular apatite. Key: Pl—Plagioclase; Am—Amphibole; Kfs—K-feldspar; Bt—Biotite; Q—Quartz; Ap—Apatite.

4. Analytical Methods

The host rock and enclave samples collected for this study were fresh, unaltered, and massive. The sampling sites were located in the middle and to the north of the Qingshanbao complex. The mafic enclave samples GS-06 and QSB-06 were collected from K-feldspar granite and adamellite, respectively. The samples were pre-treated and processed for single mineral electron probe, elemental geochemistry, and zircon chronology analyses. Single mineral electron probe analyses were conducted using a JEOL

JXA-8100 EPMA (electron probe x-ray micro-analysis) in the Key Laboratory of Nuclear Resources and Environment of East China University of Technology. Analytical conditions were set to a 15 kV voltage, 20 nA current, and 1 μm diameter beam spot. The ZAF (Z: atomic number of elements; A: absorption between elements; F: fluorescence effect) correction method was applied for the analyses. The standard samples included plagioclase for Ca, Na, Si, and Al, potassium feldspar for K, olivine for Fe and Mg, rutile for Ti and pyrophanite ($MnTiO_3$) for Mn. The relative deviation (RD) of the test data was <1%.

Elemental geochemistry analyses were performed by the Guangzhou Aoshi Analytical and Testing Co., Ltd., China. and the instrument used for the constant element test was an X-ray fluorescence spectrometer (Dutch PANalytical PW2424 model). For this test, the sample was added to a flux containing lithium nitrate, fully mixed, then melted at a high temperature. The molten material was then poured into a platinum mold to form a flat glass piece and analyzed using an X-ray fluorescence spectrometer. Simultaneously, another sample was weighed and inserted into a muffle furnace, heated at 1000 °C for 1 h and weighed again after cooling. The difference in weight before and after heating was considered as the loss on ignition. The relative deviation (RD) of the test data was <5% ($\pm$ 2.5%) and the relative error (RE) was <2% ($\pm$ 1%).

The instruments used for rare earth elements (REEs) and trace elements were an Agilent VISTA ICP-AES and a Perkin Elmer Elan 9000 ICP-MS. For these tests, the two samples were first weighed. One sample was then digested with perchloric acid ($HClO_4$), nitric acid (HNO_3), and hydrofluoric acid (HF), evaporated to near dryness, then dissolved in dilute hydrochloric acid (HCl). Plasma emission spectroscopy and plasma mass spectrometry were then used for the analysis. The other sample was added to a lithium metaborate ($LiBO_2$)/lithium tetraborate ($Li_2B_4O_7$) flux, mixed evenly and melted in a furnace at a temperature higher than 1025 °C. The melt was cooled, volumetrized with nitric acid, hydrochloric acid and hydrofluoric acid, then analyzed using a plasma mass spectrometer. According to the actual situation of the sample and the digestion effect, the comprehensive value is the final test result, according to which RD was <10% ($\pm$5%) and RE was <10% ($\pm$5%).

Zircon separating for U-Pb dating was completed at the Langfang Yuneng Rock Mineral Separation Technology Service Co., Ltd., in Hebei Province. First, rock samples were pulverized to an 80–100 mesh size and single-grain zircons with the highest purity were selected by using electromagnetic separation and flotation. The colorless, idiomorphic, subhedral, and near-equiaxed or long columnar zircons were then selected under a binocular microscope. The selected zircon grains were then adhered to a double-sided tape and epoxy resin was added to fix the crystals. After curing, half of the zircon grains were exposed by grounding and then were polished.

Zircon U-Pb dating was carried out at the State Key Laboratory for Mineral Deposits Research of Nanjing University, using an Agilent 7500a ICP-MS equipped with a New Wave Research 213 nm laser ablation system. The operating parameters of the instrument were as follows: The laser pulse frequency was 5 Hz, the laser pulse energy was in the range 0.08–0.10 mJ and the laser beam diameter was 25 μM. All measurements were adjusted according to the Australian sample zircon GEMOC GJ-1 (with a $^{207}Pb/^{206}Pb$ age of 608.5 $\pm$ 1.5 Ma) [13] and a Mud Tank zircon (749.5 $\pm$ 8.8 Ma; 2σ, *n* = 7) was used as reference standards for controlling the precision of analysis [14]. During the measurement process, the ^{204}Pb signal was close to the background, whereas the ^{206}Pb signal was much higher, indicating that the effect of common Pb on the dating was insignificant. The detailed analytical procedures were similar to those described by Jackson et al. [13]. The raw ICP-MS data were exported in the ASCII (American Standard Code for Information Interchange) format and processed using GLITTER software (Version 4.4.1) [15]. The common Pb contents were evaluated and corrected using the method described by Andersen [16].

5. Mineralogical Characteristics

Plagioclase is a common rock-forming mineral in the host complex and in the mafic enclaves. The petrographic study showed that the plagioclase within the mafic enclaves have a distinct zoning texture. Moreover, the *An* value of the plagioclase depends on the SiO_2, CaO, Na_2O, Al_2O_3, and H_2O

content of the original magma and the ratio of these elements, and can reflect the pressure conditions of the original magma [17,18]. The composition of the magma, crystallization conditions, water saturation, and other factors will therefore affect the plagioclase *An* value [19].

The locations of the EPMA point analyses on plagioclase crystals are shown in Figure 4 and the analytical results are given in Tables 1 and 2. Table 1 and Figure 4A show that the variation in *An* value from the core to the edge in the host rock is in the range of 40.29 to 22.85. The variation curve of the *An* value for this crystal is shown in Figure 4C and indicates an overall decreasing trend, suggesting that there is a gradual transition from more basic to more evolved plagioclase from the core to the edge of the crystal, meaning that the plagioclase is normally zoned. This suggests that the plagioclase could have evolved as a direct result of the progressive crystallization and evolution of the magma, producing normally-zoned plagioclase with a higher *Ab* value in the rim that grew later than in the core that grew earlier. As a result, the core is dominated by more basic plagioclase with a higher *An* value, while the margin is dominated by more evolved plagioclase with a higher *Ab* value, forming a normal annulus texture [20].

Table 1. Results of EPMA analyses of plagioclase crystals in the host rock of the Qingshanbao complex (wt %).

GS-09	Host Rock								
	1-1	1-2	1-3	1-4	1-5	1-6	1-7	1-8	1-9
SiO_2	57.31	58.08	61.55	62.25	62.49	61.55	61.30	62.10	62.13
TiO_2	0.03	-	-	-	0.02	-	-	0.03	0.01
Na2O	6.85	7.07	8.48	8.95	8.93	8.90	8.77	8.91	8.94
NiO	-	0.02	-	-	0.02	-	-	-	0.03
K_2O	0.11	0.08	0.10	0.16	0.14	0.13	0.18	0.16	0.14
MgO	-	0.01	-	-	-	-	-	-	-
FeO	0.08	0.05	0.06	0.09	0.10	-	0.04	0.07	0.04
CaO	8.46	8.03	5.31	4.85	5.12	5.34	5.33	4.93	4.90
MnO	-	0.02	-	-	-	-	-	0.02	0.01
Al_2O_3	26.99	27.06	24.55	24.03	24.42	24.41	24.45	24.32	24.08
Cr_2O_3	-	0.02	-	-	0.01	0.03	-	-	0.02
P_2O_5	0.07	0.01	0.01	-	-	-	-	-	0.02
Total	99.90	100.44	100.06	100.33	101.24	100.35	100.07	100.53	100.33
Number of ions (based on O = 8)									
Si	2.59	2.61	2.69	2.70	2.70	2.68	2.68	2.69	2.69
Ti	-	-	-	-	-	-	-	-	-
Na	0.60	0.62	0.72	0.75	0.75	0.75	0.74	0.75	0.75
Ni	-	-	-	-	-	-	-	-	-
K	0.01	-	0.01	0.01	0.01	0.01	0.01	0.01	0.01
Mg	-	-	-	-	-	-	-	-	-
Fe^{2+}	-	-	-	-	-	-	-	-	-
Ca	0.41	0.39	0.25	0.23	0.24	0.25	0.25	0.23	0.23
Mn	-	-	-	-	-	-	-	-	-
Al	1.44	1.43	1.26	1.23	1.24	1.25	1.26	1.24	1.23
Cr	-	-	-	-	-	-	-	-	-
P	-	-	-	-	-	-	-	-	-
Total	5.06	5.06	4.93	4.91	4.93	4.94	4.94	4.93	4.92
An	40.29	38.38	25.55	22.85	23.85	24.73	24.89	23.21	23.07
Ab	59.06	61.16	73.88	76.27	75.39	74.58	74.12	75.87	76.15
Or	0.65	0.47	0.57	0.88	0.76	0.69	1.00	0.92	0.77

-: Below detection; An: $Ca(AlSi_3O_8)$; Ab: $Na(AlSi_3O_8)$; Or: $K(AlSi_3O_8)$.

Table 2. Results of EPMA analyses of plagioclase crystals in the mafic enclaves of the Qingshanbao complex (wt %).

GS-06	Mafic Enclaves									
	1-1	1-2	1-3	1-4	1-5	1-6	1-7	1-8	1-9	1-10
SiO_2	60.82	63.02	62.36	61.00	62.55	62.87	61.43	64.11	60.76	62.19
TiO_2	0.01	-	-	0.02	0.01	0.01	0.01	0.01	-	0.01
Na2O	8.86	9.18	9.38	8.80	8.53	7.51	8.58	9.13	6.47	8.72
NiO	0.03	0.01	-	0.02	-	0.06	0.01	-	0.16	0.00
K_2O	0.10	0.14	0.22	0.16	0.30	0.99	0.29	0.33	0.19	0.14
MgO	-	-	0.01	0.01	0.02	0.04	0.01	0.04	0.03	0.01
FeO	0.04	0.01	0.07	0.07	0.02	0.09	0.06	0.13	0.05	0.03
CaO	5.35	4.47	4.55	5.38	4.42	6.11	5.24	4.80	2.51	5.14
MnO	-	0.01	0.01	0.02	0.02	-	-	-	-	-
Al_2O_3	24.45	23.97	23.73	24.54	23.66	23.75	24.20	24.84	24.02	24.43
Cr_2O_3	0.01	-	-	-	0.01	-	-	-	0.01	-
P_2O_5	0.02	-	-	-	0.01	-	0.04	0.05	-	-
Total	99.68	100.80	100.33	100.01	99.55	101.44	99.88	103.44	94.18	100.66
Number of ions (based on O = 8)										
Si	2.67	2.71	2.70	2.67	2.71	2.70	2.68	2.72	2.75	2.70
Ti	-	-	-	-	-	-	-	-	-	-
Na	0.75	0.77	0.79	0.75	0.72	0.63	0.73	0.75	0.57	0.73
Ni	-	-	-	-	-	-	-	-	-	-
K	0.01	0.01	0.01	0.01	0.02	0.05	0.02	0.02	0.01	0.01
Mg	-	-	-	-	-	-	-	-	-	-
Fe^{2+}	-	-	-	-	-	-	-	-	-	-
Ca	0.25	0.21	0.21	0.25	0.21	0.28	0.25	0.22	0.12	0.24
Mn	-	-	-	-	-	-	-	-	-	-
Al	1.27	1.22	1.21	1.27	1.21	1.20	1.25	1.24	1.28	1.25
Cr	-	-	-	-	-	-	-	-	-	-
P	-	-	-	-	-	-	-	-	-	-
Total	4.95	4.91	4.92	4.95	4.86	4.87	4.92	4.95	4.74	4.93
An	24.88	21.03	20.88	25.02	21.88	29.27	24.83	22.09	17.37	24.38
Ab	74.59	78.20	77.94	74.09	76.33	65.10	73.54	76.11	81.08	74.83
Or	0.54	0.77	1.18	0.89	1.79	5.63	1.63	1.80	1.54	0.80

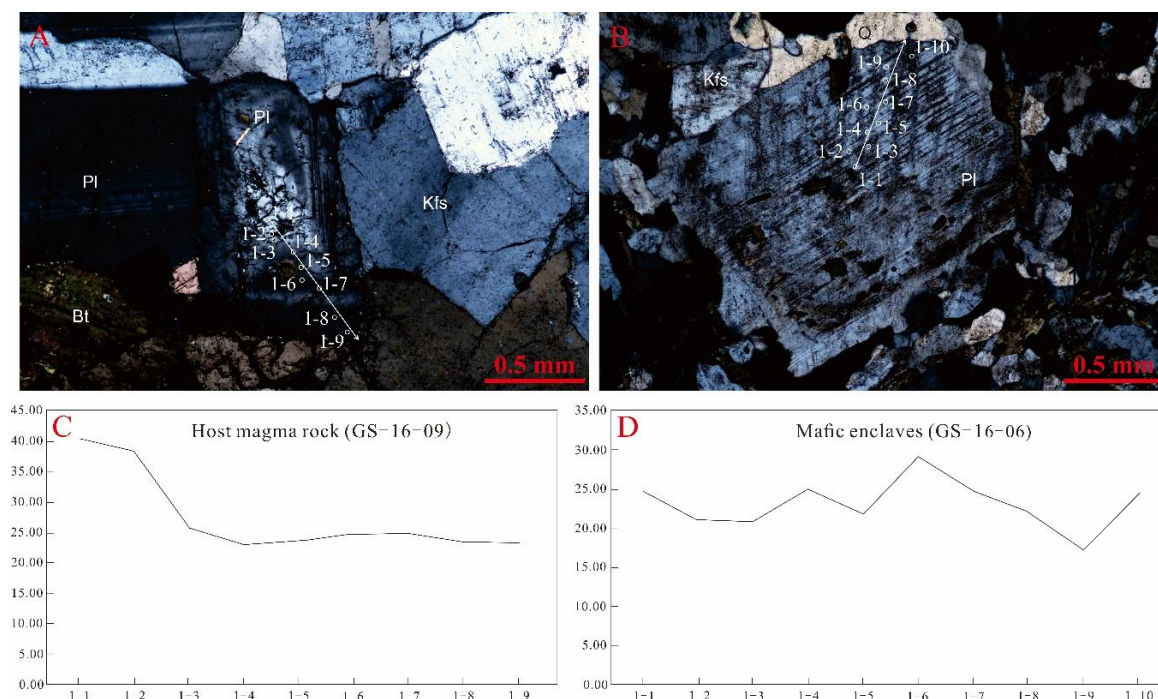-: Below detection; An: $Ca(AlSi_3O_8)$; Ab: $Na(AlSi_3O_8)$; Or: $K(AlSi_3O_8)$.

Figure 4. Locations and An values of the EPMA analyses points on the plagioclase crystals in the Qingshanbao host rock (**A**,**C**) and a mafic enclave (**B**,**D**).

The locations of the electron probe analyses and the analytical results for the plagioclase in the mafic enclaves are shown in Figure 4B and Table 2, respectively. Figure 4D shows the variation in the *An* value from the core to the rim, which is in the range of 29.27 to 17.37. The variation curve is discontinuous, which differs markedly from the smoother variation curve in the plagioclase from the host rock. This suggests that the plagioclase in the mafic enclaves is complexly zoned. The crystal shows at least three zones with alternating higher and lower *An* values. The *An* value of the inner part to the outer part of the core decreases from 24.88 to 20.88. The composition of the plagioclase on the margin also varies significantly, with the *An* value from the inner margin to the outer margin decreasing from 29.27 to 17.37. The *An* value of the most peripheral part of the crystal is 24.38. These observations clearly differ from the smoothly decreasing *An* value from the core to the edge of the plagioclase crystal measured in the host rock, indicating that the plagioclase in the dark enclave has some characteristics relating to reverse-zoning. Regarding the cause of this reverse zoning, it is generally believed that hot basic magma mixing with the cooler magma that has already crystallized the more evolved plagioclase, adds heat and causes the existing plagioclase crystals to resorb and form a dissolution texture. As a result of the mixing of the two magmas, the magma reservoir is enriched in basic elements, and more basic plagioclase then begins to crystallize on the edges of the existing, more evolved plagioclase [21]. These observations could also be related to rapid changes in temperature and pressure in the magma chamber during crystallization [22]. The inclusion, melting and mixing of limestone xenoliths in magma during its ascent may also lead to the formation of reverse-zoning. The plagioclase crystal in the dark enclave from the study area has an obvious dissolution texture and the edge is embayed (Figure 3E). The appearance of acicular apatite also implies the existence of a strong driving force for crystallization and high nucleation rates due to rapid cooling as a result of the mixing of magmas at different temperatures. The interpretation of magma mixing is therefore reasonable in this context.

6. Elemental Geochemical Characteristics

6.1. Geochemical Characteristics of Major Elements

Whole-rock geochemical results for the mafic enclaves and the host rock in the Qingshanbao complex are shown in Table 3. SiO_2 contents in the mafic enclaves are 54.05–56.54 wt % and the K_2O contents are 2.33–2.45 wt %. These values are significantly lower than those observed in the host rock, where SiO_2 content is 61.47–78.51 wt % and K_2O content is 3.58–5.10 wt % (except in two samples for which it is 1.15 and 2.04 wt %). TiO_2 contents in the mafic enclaves are 1.14–1.36 wt %, Al_2O_3 contents are 17.50–18.53 wt %, $Fe_2O_3{}^T$ contents are 6.53–6.98 wt %, Na_2O contents are 4.65–4.83 wt %, CaO contents are 5.50–5.63 wt %, MgO contents are 3.15–4.02 wt %, MnO contents are 0.14–0.19 wt %, and P_2O_5 contents are 0.61–0.70 wt %. All measured oxides are observed to be significantly higher than the corresponding components in the host rock. Except for the high Na_2O content, all other elements are consistent with the geochemical characteristics of the mafic enclaves reported in earlier studies [23–26]. On the TAS (Total Alkali-Silica) diagram shown in Figure 5A, the enclave compositions fall in the diorite and monzonite area, while the host rock compositions mainly fall in the range of granite and quartz monzonite. In general, the mafic enclaves are located near the Ir boundary and some are in the alkaline region, whereas the host rock is mainly located below the Ir boundary and is in the subalkaline region. On a SiO_2–K_2O diagram shown in Figure 5B, most of the host rock and all the mafic enclaves are in the high-K calc-alkaline series range, except for one host rock sample that falls within the low-K (tholeiitic) series range. A small number of host rock samples fall near the high-K calc-alkaline series, potassium basalt series and calc-alkaline series. On the SiO_2-AR diagram (Figure 5C), both the mafic enclaves and the host rock fall near the alkaline and calc-alkaline boundary, while the host rock is more alkaline due to the high K content. On the A/CNK–A/NK diagram (Figure 5D), the enclave samples are located in the quasi-aluminum range, while the host rock samples are located near the quasi-aluminum and peraluminum boundaries. This is consistent with the lower aluminum content of the host rock. Furthermore, on Harker diagrams (Figure 6), K_2O are positively correlated with SiO_2, while the other elements are negatively correlated with SiO_2. Overall, the mafic enclaves have intermediate-basic calc-alkaline compositions and are rich in titanium, iron, and aluminum, while the host rock has a silica-rich, calc-alkaline to alkaline composition.

Table 3. Major element content of the Qingshanbao host rock and the mafic enclaves (wt %).

| Samples | Mafic Enclaves | | Host Rock | | | | | | | | |
| | From K-Feldspar Granite | From Adamellite | K-Feldspar Granite | | | Adamellite | | | Granodiorite | | |
	GS-06	QSB-06	GS-03	GS-16	GS-27	GS-02	GS-07	GS-25	GS-04	GS-09	GS-23
SiO_2	54.05	56.54	74.33	78.51	77.16	75.37	75.41	74.58	62.79	64.93	61.47
TiO_2	1.36	1.14	0.13	0.11	0.16	0.13	0.17	0.40	0.79	0.64	0.74
Al_2O_3	18.53	17.50	13.96	11.31	12.12	13.66	13.52	12.46	17.12	16.68	16.36
TFe_2O_3	6.98	6.53	0.92	0.76	0.89	0.88	1.72	2.29	4.12	3.38	5.27
K_2O	2.45	2.33	4.78	4.44	5.10	4.64	1.15	3.58	4.00	4.83	2.04
Na_2O	4.83	4.65	4.03	2.95	3.07	3.81	4.58	3.47	4.25	4.05	4.37
CaO	5.63	5.50	0.87	0.68	0.40	0.85	2.46	1.64	3.56	2.96	4.38
MgO	4.02	3.15	0.34	0.24	0.29	0.29	0.50	0.91	1.75	1.31	2.28
MnO	0.19	0.14	0.03	0.02	0.03	0.03	0.03	0.06	0.08	0.06	0.09
P_2O_5	0.70	0.61	0.04	0.01	0.06	0.04	0.07	0.14	0.34	0.25	0.4
LOI 1000	1.59	0.90	0.88	0.83	0.80	0.95	0.59	0.91	1.32	0.73	3.08
Total	100.33	98.99	100.31	99.86	100.08	100.65	100.20	100.44	100.12	99.82	100.48
$K_2O + Na_2O$	7.28	6.98	8.81	7.39	8.17	8.45	5.73	7.05	8.25	8.88	6.41
K_2O/Na_2O	0.51	0.5	1.19	1.51	1.66	1.22	0.25	1.03	0.94	1.19	0.47
AR	1.86	1.87	3.93	4.21	4.76	3.79	2.12	3	2.33	2.65	1.89
DI	58.83	60.83	93.15	94.09	93.26	92.77	85.16	88.52	76.15	79.96	72.26
σ	4.78	3.49	2.48	1.54	1.95	2.21	1.01	1.58	3.43	3.58	2.23
A/CNK	0.89	0.87	1.04	1.04	1.07	1.06	1.02	0.99	0.96	0.97	0.94
A/NK	1.75	1.72	1.18	1.17	1.15	1.21	1.54	1.30	1.51	1.40	1.74
R1	1104	1397	2369	3127	2829	2541	3076	2822	1617	1663	1912
R2	1167	1104	383	307	295	371	553	464	805	712	901

AR (alkalinity rate) = $[Al_2O_3 + CaO + (Na_2O + K_2O)]/[Al_2O_3 + CaO − (Na_2O + K_2O)]$ (wt %); DI (differentiation index) = quartz + orthoclase + albite + nepheline + leucite + kalsilite; $\sigma = (Na_2O + K_2O)^2/(SiO_2 − 43)$ (wt %); A/CNK = $Al_2O_3/CaO + Na_2O + K_2O$; A/NK = $Al_2O_3/Na_2O + K_2O$ (Molecules number); R1 = 4Si − 11(Na + K) − 2(Fe + Ti), R2 = 6Ca + 2Mg + Al (Cation number).

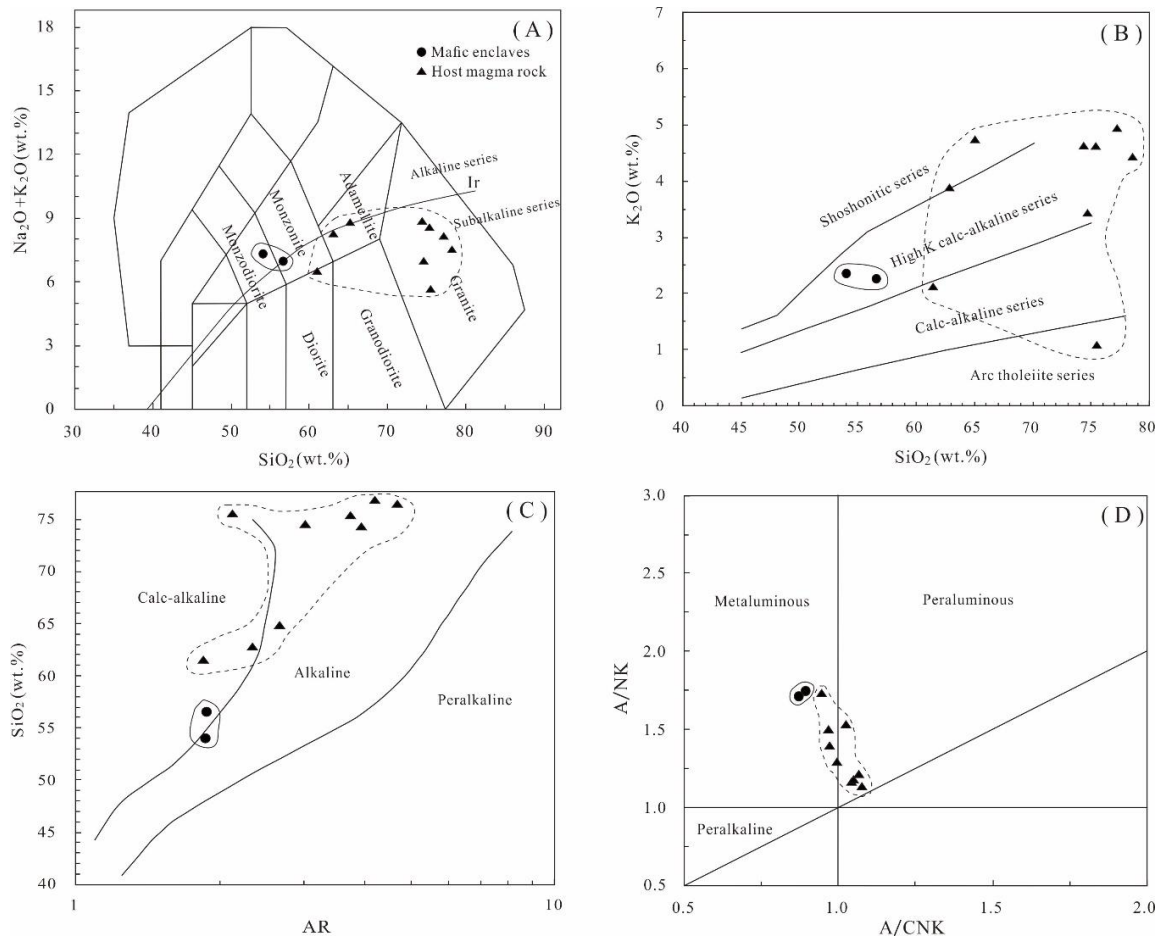**Figure 5.** Scatter plots of the geochemical characteristics of the mafic enclaves and the host rock.
(**A**) $SiO_2 - (K_2O + Na_2O)$ diagram (after Middlemost [27]). (**B**) SiO_2–K_2O diagram (after Peccerillo
and Taylor [28]). (**C**) AR–SiO_2 diagram (after Wright [29]). (**D**) A/CNK–A/NK diagram (after Maniar
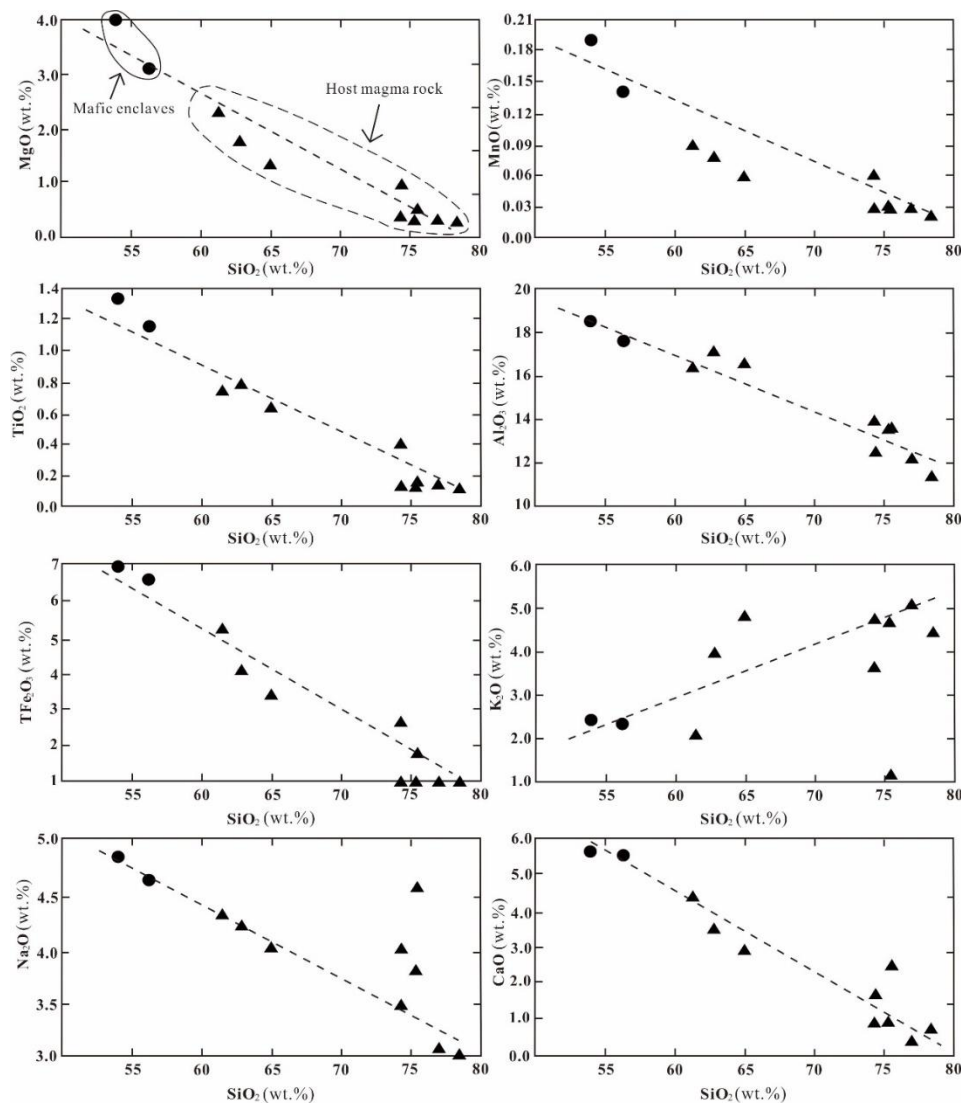and Piccoli [30]).

Figure 6. Harker diagrams showing the whole rock compositions of the mafic enclaves and the Qingshanbao host rock.

6.2. Trace Element Geochemical Characteristics

Table 4 reports the results of the trace element analyses. These results show that the mafic enclaves have a higher concentration of sulfur-transition transition elements, such as Zn, Cu, Co, Ni, Cr, and V, than the host rock. This is consistent with the general mid-base of the mafic enclaves [31]. Moreover, the spider diagram (Figure 7 [32]) shows that both the mafic enclaves and the host rock are rich in Rb, K and other lithophile elements, as well as elements such as La, Nd, and Sm. The trace element characteristics obtained from the present study are consistent with the relative depletion of Nb, Ta, P, Ti, U, and other high field strength elements observed within the predecessors of the Lushan chicken complex in Henan [33], the Qinling ring-spotted granite [34], the Karamadaz granite body in central Turkey [35], the Wulong body in South Qinling [36], and the mafic enclaves in the Yamatu body [26] in the Wolf Mountain area of North China.

Table 4. Trace element content of the mafic enclaves and the Qingshanbao host rock (wt/10^{-6}).

Samples	Mafic Enclaves		Host Rock								
	GS-06	QSB-06	GS-03	GS-16	GS-27	GS-02	GS-07	GS-25	GS-04	GS-09	GS-23
Ag **	0.05	<0.01	0.08	0.05	0.11	0.01	0.04	0.09	0.30	0.06	0.1
W	0.5	0.4	0.3	0.6	1.8	0.3	0.2	0.2	0.3	0.2	0.9
Zn *	131	102	20	13	17	16	31	49	75	59	89
Cu **	2.4	24.6	2.1	1.1	2.4	1.3	2.2	1.8	27.4	9.4	20.2
Pb **	13.9	23.9	31.3	27.4	55.5	30.8	14.7	28.0	21.4	23.0	7.6
Mo **	0.68	0.77	0.20	0.15	0.50	0.2	0.12	0.47	0.57	0.43	0.4
Ba	358	450	358	307	586	341	159.5	208	1790	1915	520
K	20,335	19,339	39,674	36,856	42,330	38,517	9545	29,714	33,200	40,089	16,934
P *	3052	2660	174	44	262	174	305	610	1482	1090	1744
As **	3.20	1.80	3.10	3.7	1.80	1.4	2.50	3.70	3.00	3.50	4.1
Be **	4.06	3.96	3.83	2.45	4.45	5.09	2.48	4.02	2.22	1.95	1.6
Ti **	8146	6829	779	659	958	779	1018	2396	4732	3834	4433
Bi **	0.33	0.27	0.11	0.11	0.28	0.19	0.10	0.10	0.25	0.07	0.04
Cd **	0.15	0.05	0.02	<0.02	0.04	0.02	0.04	<0.02	0.14	0.04	0.05
Ce	65.2	154.0	42.5	36.6	89.5	39.5	18.50	94.7	114.0	113.0	45.7
Co **	19.0	17.3	1.6	1.1	1.4	1.3	2.7	4.6	9.2	6.9	13.8
Ni **	49.4	15.5	3.0	2.1	8.0	2	4.6	6.9	15.2	8.2	13.9
Cr	57	17	3	2	11	2	4	7	10	8	26
Cs	7.53	12.40	5.96	6.96	16.95	8.97	2.89	7.48	3.42	2.55	2.58
Ga **	24.1	26.5	15.65	12.85	17.70	16	15.70	18.40	20.3	19.30	18.9
Li	55.8	75.2	35.9	12.8	53.1	35.6	19.3	64.0	27.6	21.3	69.2
Nb	19.9	47.3	9.2	11.5	14.0	11.1	2.3	25.0	22.9	19.3	10.5
Sc	12.6	13.1	2.0	2.1	2.6	1.7	1.3	4.3	5.6	4.1	8.7
Sn	4.6	3.7	1.1	2.1	0.7	1.4	0.5	2.5	2.4	1.8	1.8
V	126	121	10	8	10	10	19	29	62	49	72
Rb **	139.0	125.0	220	176.5	334	262	32.6	219	89.2	109.0	56.7
Sr **	559	668	211	80.1	147	235	345	219	749	677	313
Cs	7.53	12.40	5.96	6.51	16.95	8.32	2.89	7.48	3.42	2.55	2.5
Hf	4.7	8.1	2.2	2.2	3.7	2.3	3.9	6.0	6.7	6.5	5.7
Nb	18.7	47.3	8.3	11.5	14.7	10.7	2.4	24.7	21.3	19.6	10.5
Ta	0.92	3.74	0.79	1.11	1.43	1.03	0.11	2.03	1.48	1.30	0.64
La	44.1	58.4	25.9	17.9	53.9	21.4	12.7	53.3	69.1	72.0	33.4
Th	2.37	35.4	20.0	22.7	39.8	24.1	4.79	49.6	9.82	12.25	4.73
U	2.45	5.33	1.74	2.95	7.47	3.6	1.54	11.50	2.42	2.79	1.84
Y	18.5	46.5	4.6	15	13.4	5.1	1.8	12.2	15.6	13.8	16.3
Zr	209	319	74	55	124	71	157	216	322	304	261
Ga	23.1	26.5	14.1	12.8	16.9	15.8	14.7	18.2	19.0	19.3	18
Th/U	0.97	6.64	11.49	7.69	5.33	6.69	3.11	4.31	4.06	4.39	2.57
Nb/Ta	21.63	12.65	11.65	10.36	9.79	10.78	20.91	12.32	15.47	14.85	16.41
Nb/La	0.45	0.81	0.36	0.64	0.26	0.52	0.18	0.47	0.33	0.27	0.31
Rb/Sr	0.25	0.19	1.04	2.20	2.27	1.11	0.09	1.00	0.12	0.16	0.18

*: Test method is ICP-AES; **: Depend on content of samples and whether there is interference. The analysis data comes from ICP-AES or ICP-MS; the rest analysis data comes from ICP-MS.
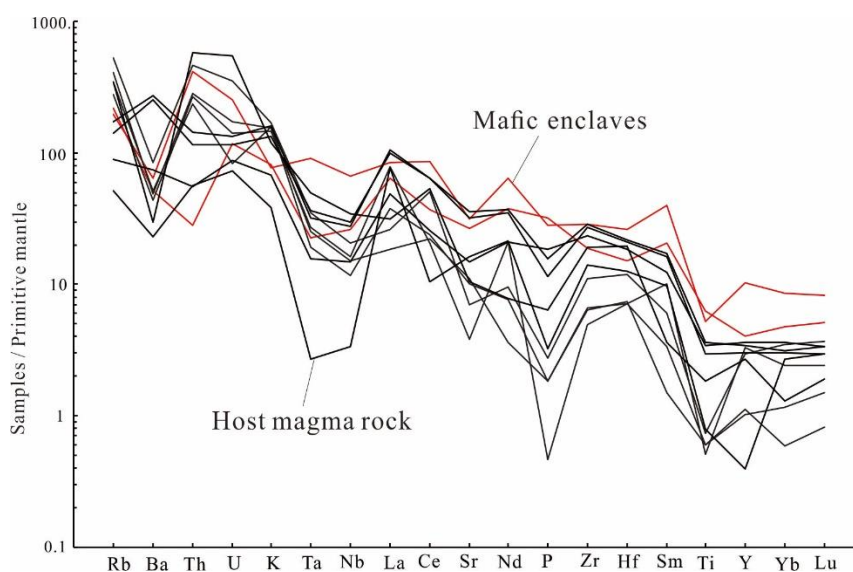

Figure 7. Primitive mantle-normalized trace element "spider" diagram of the mafic enclaves and the Qingshanbao host rock (Primitive mantle data are from Anderson [32]).

The Nb/La values for the mafic enclaves are 0.42–0.81, while those for the primitive mantle are 1.04 [37] and the Nb/La value in the lower crust is 0.4 [38]. The Nb/La values for the mafic enclaves are therefore intermediate between those of the lower crust and the primitive mantle. Similarly, the Rb/Sr values for the mafic enclaves range from 0.19 to 0.25, which lies between the values for mantle basalt (Rb/Sr = 0.025) and the continental crust (Rb/Sr = 0.24) [39]. The Nb/Ta values for the mafic enclaves (12.65–20.33) also show a partially similar trend, mostly falling between the lower crust (Nb/Ta = 8.3) and the primitive mantle (Nb/Ta = 17.4) [37,38]. This shows that the mafic enclaves record the characteristics of mafic-felsic magma mixing.

6.3. REE Geochemical Characteristics

The results of the REE analyses and the chondrite-normalized REE patterns (Table 5, Figure 8 [40]) show that both the mafic enclaves and the host rock exhibit a right-inclined trend of light rare earth element enrichment and heavy rare earth element depletion, with similar distribution patterns. Only one host rock element, Eu, exhibits a positive anomaly (δEu = 1.92), while all other samples measured in the host rock and mafic enclaves have similar weak-medium negative anomalies (mafic enclaves: δEu = 0.66–0.98, host rock: δEu = 0.43–0.90), which is similar to the weak negative anomaly of Eu in the mafic enclaves reported in previous studies [26,36,41–43]. Ce did not show any obvious anomaly (mafic enclaves: δCe = 1.06–1.07, host rock: δCe = 0.89–1.05). Furthermore, the total REE values in the mafic enclaves are higher than those of the host rock, which further implies that the mafic enclaves are not products of early crystallization differentiation of the host magma. This is because the REE are strongly incompatible elements, therefore if the mafic enclaves were the products of early crystallization differentiation of granitic magma, the total amount of REE in those enclaves would be lower than the corresponding value in the host rock, and the distribution curve would also be located below the host rock curve [44] but this is not the case.

Table 5. REE content of the Qingshanbao complex and their mafic enclaves (wt/10^{-6}).

Samples	Mafic Enclaves				Host Rock						
	GS-06	QSB-06	GS-03	GS-27	GS-16	GS-07	GS-25	GS-02	GS-04	GS-09	GS-23
La	44.1	58.4	25.9	53.9	17.9	12.7	53.3	21.4	69.1	72.0	33.4
Ce	105.5	154.0	40.4	87.7	36.4	19.9	100.0	39.6	145.5	142.0	69
Pr	13.25	21.4	3.48	8.97	3.73	1.65	9.18	3.41	15.25	14.20	7.6
Nd	51.1	87.3	10.4	28.2	12.8	4.9	29.2	10.6	50.4	47.5	28.3
Sm	9.23	17.80	1.50	4.49	2.7	0.67	4.28	1.61	7.55	7.17	5.47
Eu	2.67	3.36	0.39	0.55	0.45	0.38	0.82	0.37	1.73	1.62	1.45
Gd	6.84	12.25	1.04	3.03	2.44	0.50	3.15	1.15	5.12	4.79	4.86
Tb	0.92	1.71	0.16	0.39	0.42	0.06	0.42	0.17	0.66	0.61	0.69
Dy	5.01	9.25	0.81	2.24	2.63	0.33	2.26	0.89	3.49	3.19	4.05
Ho	0.87	1.75	0.16	0.41	0.53	0.07	0.41	0.19	0.65	0.59	0.78
Er	2.53	4.69	0.46	1.20	1.58	0.21	1.22	0.53	1.66	1.56	2.06
Tm	0.38	0.65	0.08	0.18	0.25	0.04	0.19	0.09	0.25	0.23	0.28
Yb	2.36	4.19	0.57	1.19	1.72	0.29	1.32	0.64	1.55	1.48	1.79
Lu	0.38	0.61	0.11	0.18	0.27	0.06	0.22	0.14	0.25	0.22	0.25
Y	18.5	46.5	4.6	13.4	15	1.8	12.2	5.1	15.6	13.8	16.3
ΣREE	245.14	377.36	85.46	192.63	83.82	41.76	205.97	80.79	303.16	297.16	159.98
LREE	225.85	342.26	82.07	183.81	73.98	40.20	196.78	76.99	289.53	284.49	145.22
HREE	19.29	35.10	3.39	8.82	9.84	1.56	9.19	3.8	13.63	12.67	14.76
LREE/HREE	11.71	9.75	24.21	20.84	7.52	25.77	21.41	20.26	21.24	22.45	9.84
La$_N$/Yb$_N$	13.40	10.00	32.59	32.49	7.46	31.41	28.96	23.98	31.98	34.90	13.38
δEu	0.98	0.66	0.90	0.43	0.53	1.92	0.65	0.79	0.80	0.80	0.84
δCe	1.06	1.07	0.90	0.89	1.04	0.92	1.02	1.03	1.05	1.02	1.02

Test method is ICP-MS.REE: Sum of light rare earth elements; HREE: Sum of heavy rare earth elements. La$_N$ = La/La*; Yb$_N$ = Yb/Yb*; δEu = (Eu/Eu*)/[(Sm/Sm* + Gd/Gd*)/2]; δCe = (Ce/Ce*)/[(La/La* + Pr/Pr*)/2], (wt 10^{-6}). La*, Yb*, Eu*, Sm*, Gd*, Ce*, La*, Pr*: Elements content in chondrite.
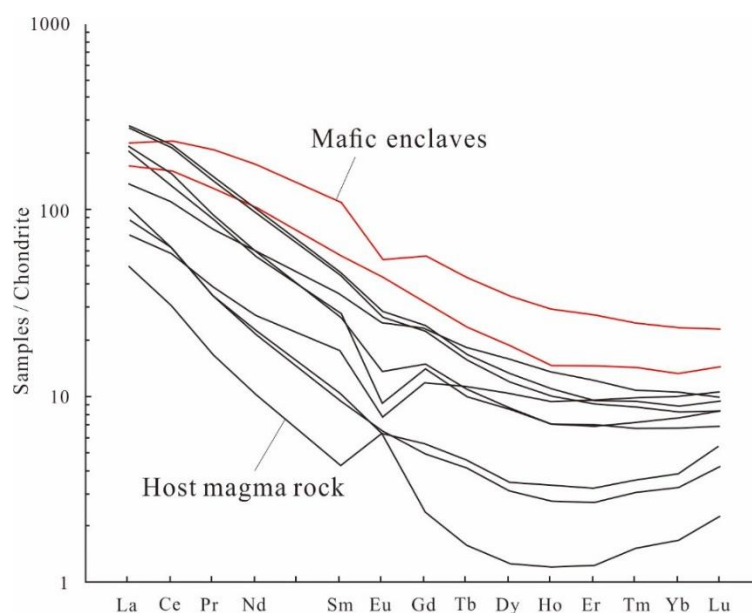
Figure 8. Chondrite-normalized rare earth elements (REE) patterns of the mafic enclaves (pink) and the Qingshanbao host rock (grey) (Chondrite data after Taylor and McLennan [40]).

7. Zircon U-Pb Chronology

Zircon is a colorless euhedral-subhedral shaped columnar crystal with an aspect ratio of 1.5–2.5, with a distinct oscillating ring structure under cathodoluminescence. The Th/U ratios of the two groups of zircons are high, with Th/U ratios of the mafic enclaves in the range of 0.69 to 2.88, and the Th/U ratios in the host rocks in the range of 0.57 to 1.76. These ratios are typical for magmatic zircon as they are greater than 0.4 [45,46]. The dating data for the zircons is given in Table 6 and shows that the ^{232}Th content of the mafic enclaves is in the range of 51 ppm to 408 ppm, the ^{238}U content for the enclaves is in the range of 61 ppm to 303 ppm, and the weighted average age of ^{206}Pb/^{238}U is 431.8 ± 5.2 Ma (MSWD = 1.5, *n* = 14) (Figure 9). Similarly, the ^{232}Th content of the host rock is in the range of 250 ppm to 1079 ppm, the ^{238}U content is in the range of 165 ppm to 1113 ppm (Table 7), and the weighted average age of ^{206}Pb/^{238}U is 432.8 ± 4.2 Ma (MSWD = 1.7, *n* = 16) (Figure 10). These results can be used to represent the crystallization time of the mafic enclaves and the host rock. The weighted average age (441.6 ± 4.2 Ma, MSWD = 1.4, *n* = 14) of zircons from coarse-grained K-feldspar granites in the Qingshanbao complex is consistent with the weighted average age (444 ± 2 Ma, MSWD = 0.25, *n* = 13) of zircons from the Mengjia Dawan granite in the Qingshanbao complex measured in a previous study [9] and is within the error range. This indicates a formation during the early Silurian Period, which coincides with the age of the collision of the Alashan Block (late Caledonian) [47].

Table 6. Results of zircon U-Pb age analysis of the mafic enclaves in the Qingshanbao complex.

Analysis	^{232}Th	^{238}U	Th/U	Isotopic Ratios						Isotopic Ages (Ma)					
				^{207}Pb/^{206}Pb		^{207}Pb/^{235}U		^{206}Pb/^{238}U		^{207}Pb/^{206}Pb		^{207}Pb/^{235}U		^{206}Pb/^{238}U	
	(ppm)	(ppm)		1sd (±%)		1sd (±%)		1sd (±%)		1sd (±%)		1sd (±%)		1sd (±%)	
GS06-1	408	231	1.77	0.06313	0.00232	0.59519	0.02093	0.06838	0.00119	713	80	474	13	426	7
GS06-2	230	164	1.40	0.05842	0.00229	0.54318	0.02048	0.06744	0.00118	546	88	441	13	421	7
GS06-3	399	232	1.72	0.05377	0.00189	0.49820	0.01694	0.06720	0.00110	361	81	410	11	419	7
GS06-4	407	303	1.34	0.05747	0.00198	0.53519	0.01773	0.06755	0.00113	510	78	435	12	421	7
GS06-5	393	158	2.49	0.05752	0.00300	0.55447	0.02771	0.06992	0.00143	512	118	448	18	436	9
GS06-6	159	164	0.97	0.05379	0.00208	0.51380	0.01924	0.06929	0.00117	362	89	421	13	432	7
GS06-7	51	73	0.69	0.05353	0.00390	0.52657	0.03716	0.07135	0.00168	351	168	430	25	444	10
GS06-8	223	121	1.84	0.05477	0.00259	0.53205	0.02429	0.07046	0.00134	403	109	433	16	439	8
GS06-9	175	61	2.88	0.05503	0.00402	0.53707	0.03802	0.07079	0.00166	413	168	436	25	441	10
GS06-10	257	167	1.54	0.05673	0.00183	0.55337	0.01734	0.07075	0.00113	481	73	447	11	441	7
GS06-11	391	163	2.40	0.05556	0.00186	0.54858	0.01779	0.07161	0.00117	435	76	444	12	446	7
GS06-12	178	113	1.58	0.06000	0.00350	0.57256	0.03205	0.06922	0.00153	604	130	460	21	431	9
GS06-13	298	118	2.53	0.05528	0.00221	0.53483	0.02071	0.07018	0.00123	424	91	435	14	437	7
GS06-14	247	242	1.02	0.06285	0.00159	0.59355	0.01451	0.06850	0.00106	703	55	473	9	427	6

1sd: 1 standard deviation.

Table 7. Results of zircon U-Pb age analysis of the host magma (monzogranite) from the Qingshanbao complex.

| Analysis	^{232}Th	^{238}U	Th/U	Isotopic Ratios						Isotopic Ages (Ma)					
				^{207}Pb/^{206}Pb		^{207}Pb/^{235}U		^{206}Pb/^{238}U		^{207}Pb/^{206}Pb		^{207}Pb/^{235}U		^{206}Pb/^{238}U	
	(ppm)	(ppm)		1sd (±%)		1sd (±%)		1sd (±%)		1sd (±%)		1sd (±%)		1sd (±%)	
qsb-15-1	569	743	0.77	0.06189	0.00303	0.5763	0.02693	0.06753	0.00099	670	108	462	17	421	6
qsb-15-2	1079	1113	0.97	0.05836	0.00112	0.5598	0.01188	0.0696	0.00105	543	43	451	8	434	6
qsb-15-3	250	165	1.52	0.05721	0.00146	0.54353	0.01444	0.06892	0.00105	500	58	441	9	430	6
qsb-15-4	681	769	0.89	0.05962	0.00112	0.56903	0.01177	0.06925	0.00102	590	42	457	8	432	6
qsb-15-5	694	815	0.85	0.06133	0.00108	0.56913	0.01115	0.06733	0.00097	651	39	457	7	420	6
qsb-15-6	338	431	0.78	0.06617	0.00125	0.63676	0.01311	0.06982	0.00101	812	40	500	8	435	6
qsb-15-7	754	429	1.76	0.0618	0.00112	0.58593	0.01164	0.06879	0.00098	667	40	468	7	429	6
qsb-15-8	375	252	1.49	0.0577	0.00119	0.57422	0.01266	0.07221	0.00105	518	46	461	8	449	6
qsb-15-9	417	585	0.71	0.06378	0.00121	0.60421	0.01245	0.06874	0.00098	734	41	480	8	429	6
qsb-15-10	609	795	0.77	0.05802	0.00118	0.57858	0.01296	0.07242	0.00111	531	46	464	8	451	7
qsb-15-11	533	838	0.64	0.05798	0.00125	0.55667	0.01298	0.06971	0.00107	529	48	449	8	434	6
qsb-15-12	491	429	1.15	0.0589	0.00139	0.57282	0.01438	0.0706	0.00109	563	53	460	9	440	7
qsb-15-13	446	465	0.96	0.05807	0.00122	0.55623	0.0126	0.06949	0.00104	532	47	449	8	433	6
qsb-15-14	346	602	0.57	0.05628	0.0012	0.53889	0.01239	0.06947	0.00104	463	48	438	8	433	6
qsb-15-15	630	840	0.75	0.06396	0.0013	0.61097	0.01347	0.06929	0.00103	740	44	484	8	432	6
qsb-15-16	609	808	0.75	0.06023	0.00126	0.57104	0.01288	0.06877	0.00103	612	46	459	8	429	6
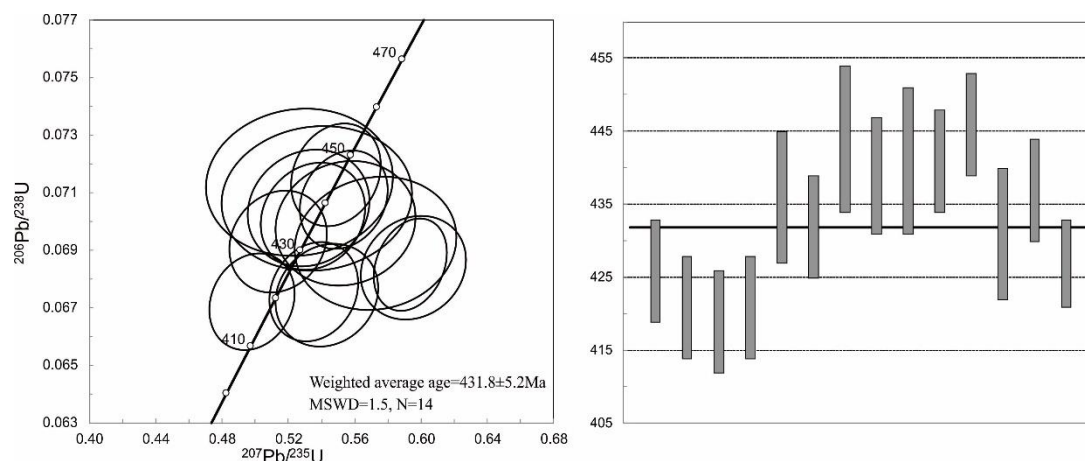
Figure 9. Zircon U-Pb Concordia ages diagram of the mafic enclaves in the Qingshanbao complex.
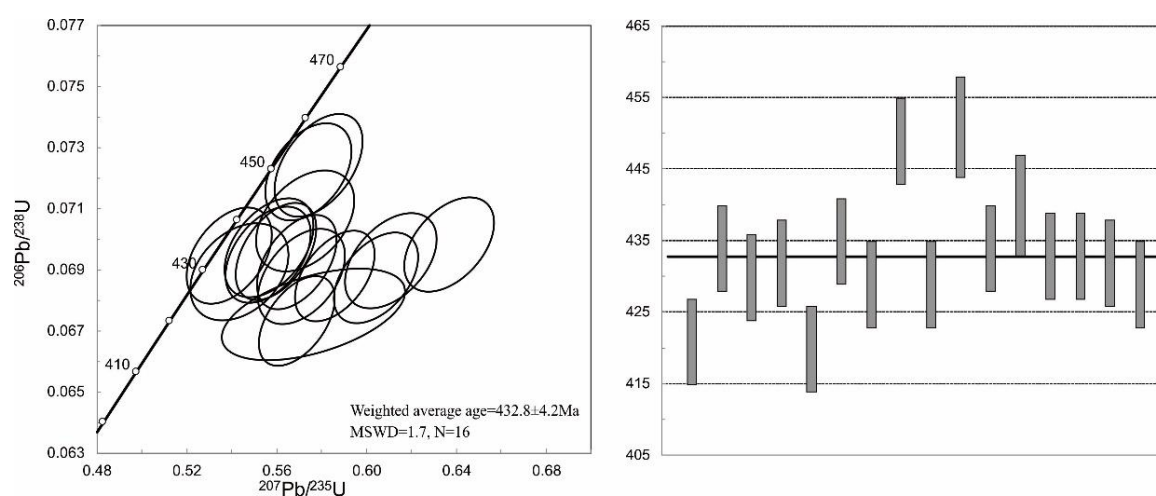

Figure 10. Zircon U-Pb Concordia ages diagram of the host magma (monzogranite) in the Qingshanbao complex.

8. Discussion

8.1. Origin of the Mafic Enclaves

There are primarily three possible explanations for the formation of mafic enclaves in granite rock bodies: (1) Differentiation of basic magma [48–50]; (2) refractory residual or xenolith in the magma source area [51,52]; (3) mixing of basic and evolved magma [8,53]. The Qingshanbao complex is dominated by granitoids and only the late basic rocks are penetrated into the early K-feldspar granite, granodiorite, and monzonitic granite. Moreover, there are no large exposures of basic rocks. An origin related to evolution from the crystallization differentiation process of basic magma is therefore very unlikely. In addition, the mafic enclaves have a typical magmatic texture, with a magmatic zircon crystal age of 431.8 ± 5.2 Ma (MSWD = 1.5, *n* = 14), while the host magma (adamellite) zircon crystal age is 432.8 ± 4.2 Ma (MSWD = 1.7, *n* = 16). These ages are almost identical within the error range and indicate that the complex is not a refractory residue or a surrounding rock trapped in the magma source area. The mafic enclaves within the Qingshanbao complex were therefore formed by the mixing of basic and more evolved magma under similar pressure conditions. We review the evidence for this below.

(1) The mafic enclaves of the Qingshanbao complex are ellipsoidal, lenticular, or globular in shape within the host rock (Figure 2). This is considered to indicate a fluid state between the two magmas and is a clear sign of mixing [48,54]. In addition, the boundary between the mafic

enclaves and the host rock is straight, clear, and cut-off type [55] and is therefore not likely to be related to a melting relationship between the two magmas. However, dark borders and light-colored edges are also visible at some boundaries between the enclaves and the granite. The dark edges are located at the inner contact between the mafic enclaves and the host rock and are the result of the aggregation of femic minerals in the mafic enclaves. The light-colored edges are the result of the outward migration of elements from the enclaves.

(2)   The mafic enclaves of the Qingshanbao complex are fine-grained semi-automorphic granular structures with typical magmatic textural features (Figure 3A). Kim et al. [56] noted that the grain size and fine-grained texture of the enclaves indicate that the mafic magma invaded the granite magma in an approximately liquid state. Microscopically, plagioclase shows obvious dissolution textures with embayed edges (Figure 3E) and reverse zoning, which could be related to the heating of a cooler, partially crystallized felsic magma by the hot basic magma. In addition, the rapidly crystallized ferromagnesian minerals in the rapidly cooled enclaves are encapsulated by larger plagioclase crystals formed at a later stage, under lower nucleation rates and high growth rates (Figure 3E). The rounded quartz crystals present as inclusions in some plagioclase crystals may represent quartz captured from the host magma (Figure 3D). Both the above scenarios indicate a magma mixing origin for these enclaves.

(3)   Needle-shaped apatite is widely present in the mafic enclaves (Figure 3F) and has an aspect ratio that varies between 5 and 15. It can be distinguished from the short columnar apatite (with a length to width ratio of 3–4) in normal granite and is a recognized standard mineral, suggesting magma mixing. Acicular apatite is commonly considered as a crystalline product obtained when high-temperature basic magma is injected into a lower temperature, more evolved magma during mixing, causing a sudden drop in the temperature of the basic magma [57,58]. Wyllie et al. [59] also proved through experiments that acicular apatite is formed in a "quenching" environment when the magma is rapidly cooled, which represents important evidence for the magma mixing process.

(4)   Electron probe analyses showed that the plagioclase in the host rock is normally zoned and formed due to the normal crystallization of the magma. However, the plagioclase in the mafic enclaves shows reverse-zoning characteristic of a chilled basic magma. Overall, the resident felsic magma with partially crystallized plagioclase with more evolved compositions became heated during mixing, and the basicity of the magma also increased due to the compositional mixing of the two magmas. More basic plagioclase then crystallized on the periphery of the more evolved plagioclase cores.

(5)   In terms of geochemical characteristics, the Harker diagrams showing the compositions of the mafic enclaves and the host rock exhibit a good linear relationship. A linear relationship within Harker diagrams was generally interpreted as either being due to crystallization differentiation, residual body incompatibility, or magma mixing [23,60–62]. However, crystallization differentiation generally shows a curved distribution [23,36,63]. Most of the residual body that was not extensively mixed comprises S-type granite [55], and is closed by the northern part of the area. The resulting tectonic setting of continent collisional orogeny does not match [47,64,65]. Thus, only in the case of magma mixing could the Harker diagrams of the dark enclave and host rock compositions exhibit such a linear relationship. In addition, compared with the host rock, the mafic enclaves are richer in Fe, Mg, lean Si, K, and the ratios of trace elements such as Nb/La, Rb/Sr, and Nb/Ta lie between the ratios of the crust and the mantle, suggesting that the mafic enclaves contain iron and resulted from a combination of mafic and felsic magma. In terms of REE characteristics, both the mafic enclaves and the host rock exhibit a right-inclined trend of light rare earth element enrichment and heavy rare earth element loss, and the distribution patterns are similar. The total amount of REEs in the mafic enclaves is higher than the value for the corresponding element in the host rock and this suggests that the mafic enclaves are not the products of early crystallization differentiation of the host magma. These

geochemical characteristics show that the mafic enclaves formed by magma mixing, rather than from granitic magma crystallization differentiation and other origins.

(6) In terms of crystallization age of the Qingshanbao complex, Wei et al. [9] reported a U-Pb age of zircons in the Mengshan Dawan granite of Qingshanbao as 444 ± 2 Ma (MSWD = 0.25, *n* = 13) and Liu et al. (to be published) obtained a zircon U-Pb age of the medium-coarse grained K-feldspar granite in the Qingshanbao complex as 441.6 ± 4.2 Ma (MSWD = 1.4, *n* = 14). In the present study, the LA-ICP-MS U-Pb dating results for magmatic zircons in the mafic enclaves and host rocks yielded ages of 431.8 ± 5.2 Ma (MSWD = 1.5, *n* = 14) and 432.8 ± 4.2 Ma (MSWD = 1.7, respectively, *n* = 16), respectively. The two ages are not only highly consistent, but also approximately consistent with the crystallization age of the complex reported in previous studies. If the mafic enclaves were traps or residues, they would have formed earlier than the host rock. Thus, only mafic enclaves formed as a result of magma mixing allow the crystallization age to be consistent with, or very close to, the age of the host rock.

8.2. Tectonic Significance

We now consider the formation, evolution, emplacement, and crystallization of the host rock and the mafic enclaves in relation to the specific geotectonic environment. Most of the K-feldspar crystals and monzonitic granite in the Qingshanbao granitic body contain dark microgranular enclaves, which show the characteristics of magma mixing. This is of great significance for understanding the nature and evolution processes of the magma source in the study area and to deduce the tectonic background and evolution. The existence of a large number of mafic enclaves also implies the participation of mantle-derived basic magma in the formation of the host rock. The presence of basic rocks characterized by dark minerals is generally associated with the partial melting of the mantle in an extensional environment [66,67]. Some researchers believe that the mafic enclaves represent magma underplating and magma mixing [68–70], while others believe that mafic enclaves reflect a dynamic background of subduction and generally attest to the presence of a subduction zone arc or active continental margin [71,72]. Overall, the intrusion of mantle-derived magma into the lower crust is prone to occur within the dynamics of an extensional or subduction environment. When this occurs, the high-temperature mantle-derived basic magma induces the eutectic components of the lower crust to melt through heat and volatile transfer. The crust continues to melt due to the continuous upward infiltration and penetration of basic magma, which promotes the mixing of the basic and more silicic magmas [73]. During the ascent of the more felsic magma resulting from crustal melting, a reservoir of this more silicic magma may form. Basic magma entering this reservoir at a late stage may be dispersed into various parts of the magma chamber in the form of enclaves due to magmatic convection before complete assimilation occurs. These enclaves may finally crystallize within the surrounding host magma to form mafic enclaves within a granitic host rock. Some researchers have also suggested that the basic magma that was not involved in the magma mixing may be distributed beneath the evolved magma and is not exposed at the surface [74]. This is also consistent with the occurrence of basic rock in the Qingshanbao area from the same period within host rock bodies such as K-feldspar granite and monzonitic granite.

Previous studies have noted that the granite in the area of the Longshou Mountain formed a tectonic thermal event caused by the collision of the Alashan Block, which was caused by the closure of the Qilian Ocean [64]. The Qingshanbao complex belongs to the granite group of the Longshou Mountain uplift zone and is also closely related to the evolution of plate tectonic movements. Xu et al. [75] proposed that the initial timing of the continent-continent collision after the closure of the Qilian Ocean was between 467–450 Ma. Xia et al. [76] proposed that the initial timing of the continent–continent collision after the closure of the Qilian Ocean was around 416 Ma (late Silurian to early Devonian) from the collisional compression stage to the extensional stage. Wei et al. [9] proposed that the Qingshanbao granite was formed in the same collisional environment, and the initial collision after the closure of the North Qilian Ocean was delayed to 444 ± 2 Ma. Through zircon geochronology

and Sr-Nd isotope geochemistry, the author suggested that, except for the late fine-grained granites in the Qingshanbao complex, the other granite-like rock bodies formed within the same collision stage of the Alashan Block. They proposed that the late fine-grained granites were formed during the stretching stage after the collisional orogeny (to be published). Combining the previous research results and the observation of a large number of mafic enclaves in the Qingshanbao complex, it can be considered that there was a northward subduction in the northern Qilian Ocean in the late upper Ordovician Period. During this subduction process, the fluid in the subduction zone metasomatized the mantle wedge, resulting in partial melting to form basic magma. This high-temperature basic magma induced partial melting of the lower crustal material to form more silicic magma during underplating, and this more evolved magma mixed with the rising basic magma. When two types of magma with different temperatures, compositions, and viscosity are mixed, some of the hotter basic magma will typically cool rapidly to form mafic enclaves, which are then dispersed throughout the more silicic magma due to convection, forming rounded and lenticular shapes. After subduction, the Qilian Ocean finally closed and triggered a continent–continent orogeny due to the arrival of the Alashan Block. In addition, studies have shown that the Qingshanbao complex, except the fine-grained granite, is mainly an I-type granite, which are generally formed in an island arc or active continental margin environment, which corresponds to the location where lithospheric plates subduct and collision occurs [77]. Thus, we conclude that the Qingshanbao complex was mainly formed during the collisional orogeny related to the closure of the Qilian Ocean and the arrival of the Alashan Block. At this time, the underplating of mantle-derived magma caused the melting of the ancient basement crustal material and eventually led to the mixing of crust-derived and mantle-derived magma, to form the mafic enclaves. Previous studies have shown that the mixing of crust and mantle sources played an important role in the formation of the Qingshanbao complex.

9. Conclusions

(1) Electron microprobe analyses show that the plagioclase in the host rock is normally zoned, while the plagioclase in the mafic enclaves shows discontinuous zoning and shows instances of reverse-zoning.

(2) The zircon LA-ICP-MS U-Pb analyses indicate that mafic enclaves and host rocks formed at 431.8 ± 5.2 Ma (MSWD = 1.5, $n = 14$) and 432.8 ± 4.2 Ma (MSWD = 1.7, $n = 16$), which coincide with the timing of the collision of the Alashan Block (late Caledonian).

(3) Mafic enclaves were formed in a collisional orogenic setting resulting from mixing of the crust-derived and mantle-derived magmas in a subduction–collision setting in the Alashan Block in the early Silurian.

Author Contributions: Conceptualization and Methodology, W.L.; Software, Y.N.; Formal Analysis, K.W.; Investigation, G.W.; Data Curation, W.G.; Writing-Review & Editing, J.P.; Project Administration, X.L.

References

1. Castro, A.; Morenoventas, I.; Delarosa, J.D. Multistage crystallization of tonalitic enclaves in granitoid rocks (Hercynian belt, Span): Implications for magma mixing. *Geol. Rundsch.* **1991**, *80*, 109–120. [CrossRef]

2. Barbarin, B.; Didier, J. Genesis and evolution of mafic microgranular enclaves through various types of interaction between coexisting felsic and mafic magmas. *Trans. R. Soc. Edinb. Earth Sci.* **1992**, *83*, 145–153. [CrossRef]

3. Wiebe, R.A.; Smith, D.; Sturm, M. Enclaves in the Cadillac mountain granite (coastal Maine): Samples of hybrid magma from the base of the chamber. *J. Petrol.* **1997**, *38*, 393–423. [CrossRef]

4. Wang, T.; Wang, X.X.; Li, W.P. Evaluation of multiple emplacement mechanisms of Huichizi granite pluton, Qinling orogenic belt, central China. *J. Struct. Geol.* **2000**, *22*, 505–518. [CrossRef]

5. Wilcox, R.E. The idea of magma mixing: History of a struggle for acceptance. *J. Geol.* **1999**, *107*, 421–432. [CrossRef]

6. Ma, X.X.; Joseph, G.M.; Xu, Z.Q.; Zhao, Z.B. Evidence of magma mixing identified in the Early Eocene Caina pluton from the Gangdese Batholith, southern Tibet. *Lithos* **2017**, *278–281*, 126–139. [CrossRef]

7. Ma, X.H.; Chen, B.; Yang, M.C. Magma mixing origin for the Aolunhua porphyry related to Mo–Cu mineralization, eastern Central Asian Orogenic Belt. *Gondwana Res.* **2013**, *24*, 1152–1171. [CrossRef]

8. Didier, J.; Barbarin, B. *Enclaves and Granite Petrology*; Elsevier Science Publishers: Amsterdam, The Netherlands, 1991.

9. Wei, Q.Q.; Hao, L.B.; Lu, J.L.; Zhao, Y.Y.; Zhao, X.Y.; Shi, H.L. LA-MC-ICP-MS zircon U-Pb age and its geological significance in Hexibao granite, Gansu Province. *Bull. Mineral. Geochem.* **2013**, *32*, 729–735.

10. Zhao, R.Y.; Chen, Y.J.; Wu, B.; Wang, G. A metallogenic model of the sodic-metasomatic type uranium deposit in the Jiling area of Longshoushan, Gansu Province. *Geol. Explor.* **2013**, *49*, 67–74.

11. Chen, Y.J.; Fu, C.M.; Wang, W.; Li, T. Discussion on the genesis and prospecting direction of the Jinbiansi uranium deposit in Gansu. *J. Mineral.* **2013**, 747–748.

12. Song, S.G.; Niu, Y.L.; Su, L.; Xia, X.H. Tectonics of the North Qilian orogen, NW China. *Gondwana Res.* **2013**, *23*, 1378–1401. [CrossRef]

13. Jackson, S.E.; Pearson, N.J.; Griffin, W.L.; Belousova, E.A. The application of laser ablation-inductively coupled plasma-massspectrometry to in situ U–Pb zircon geochronology. *Chem. Geol.* **2004**, *211*, 47–69. [CrossRef]

14. Black, L.; Gulson, B. The age of the Mud Tank carbonatite, Strangways Range, Northern Territory. *BMR J. Aust. Geol. Geophys.* **1978**, *3*, 227–232.

15. Van Achterbergh, E.; Ryan, C.; Jackson, S.; Griffin, W. Data reduction software for LA-ICP-MS. Laser-Ablation-ICPMS in the earth sciences principles and applications. *Miner. Assoc. Can.* **2001**, *29*, 239–243.

16. Andersen, T. Correction of common lead in U-Pb analyses that do not report 204Pb. *Chem. Geol.* **2002**, *192*, 59–79. [CrossRef]

17. Panjasawatwong, Y.; Danyushevsky, L.V.; Crawford, A.J.; Harris, K.L. An Experimental study of the effects of melt composition on Plagioclase-melt equilibria at 5 and 10 kbar: Implications for the origin of magmatic high-an plagioclase. *Contrib. Mineral. Petrol.* **1995**, *118*, 420–432. [CrossRef]

18. Guo, F.; Li, H.X.; Fan, W.M.; Li, J.; Zhao, L.; Huang, M.; Xu, W.L. Early Jurassic subduction of the paleo-pacific ocean in NE China: Petrologic and geochemical evidence from the Tumen mafic intrusive complex. *Lithos* **2015**, *224–225*, 46–60. [CrossRef]

19. Feng, G.Y.; Liu, W.; Niu, X.L.; Yang, J.Y. Chronology, geochemistry and petrogenesis of the Early-Middle Permian mafic intrusive rocks in the Zhangguangcailing block. *Earth Sci.* **2018**, *43*, 1293–1310.

20. Xie, L.; Wang, D.Z.; Wang, Y.C.; Qiu, J.S.; Chen, X.M. Quartz diorite enclaves in the Putuo granit complex in Zhejiang: A study of the complex annulus inside the plagioclase and a history of magma mixing. *J. Rock* **2004**, *20*, 96–107.

21. Niu, Z.J.; Liu, Y.; Di, Y.J. Characteristics and geological significance of the plagioclase belt in the Mesozoic coarse-rock in the Wudaogou area, Daxing'anling. *J. Rock Mineral.* **2014**, *33*, 102–108.

22. Smith, R.K.; Lofgren, G.E. Ananalytical and experimental study of zoning in plagioclase. *Lithos* **1983**, *16*, 153–168. [CrossRef]

23. Choe, W.H.; Jwa, Y.J. Petrological and geochemical evidences for magma mixing in the Palgongsan rock mass. *Geosci. J.* **2004**, *8*, 343–354. [CrossRef]

24. Barbarin, B. Mafic magmatic enclaves and mafic rocks associated with some granitoids of the central Sierra Nevada batholith, California: Nature, origin, and relations with the hosts. *Lithos* **2005**, *80*, 155–177. [CrossRef]

25. Zhao, H.D.; Han, Z.Z.; Zhao, H.B.; Niu, Y.H.; Ma, L.L. Characteristics and genesis of enclaves in the riprap granite in northeastern Inner Mongolia. *Geol. Bull.* **2005**, *24*, 841–847.

26. Zhang, J.J.; Wang, T.; Zhang, Z.C.; Tong, Y.; Zhang, L.; Shi, X.J.; Guo, L.; Li, S.; Zeng, T. The magmatic mixing genesis of the Yamatu rock mass in the Bayinuoergong-Wolshan area in the western part of the northern margin of the North China block: Lithofacies and elemental geochemical evidence. *Geol. Rev.* **2012**, *58*, 53–66.

27. Middlemost, E.A.K. Naming materials in the magma/igneous rock system. *Earth-Sci. Rev.* **1994**, *37*, 215–224. [CrossRef]

28. Peccerillo, A.; Taylor, S.R. Geochemistry of Eocene calc-alkaline volcanic rocks from the Kastamonu area, Northern Turkey. *Contrib. Mineral. Petrol.* **1976**, *58*, 63–91. [CrossRef]

29. Wright, J.B.A. Simple alkalinity ratio and its application to question of non-orogenic granite geneses. *Geol. Mag.* **1969**, *106*, 370–384. [CrossRef]

30. Maniar, P.D.; Piccoli, P.M. Tectonic discrimination of granitoids. *Geol. Soc. Am. Bull.* **1989**, *10*, 635–643. [CrossRef]

31. Fu, Q.; Ge, W.S.; Wen, C.S.; Cai, K.Q.; Li, S.F.; Zhang, Z.W.; Li, X.F. Geochemical Characteristics and Genesis Analysis of Guangxi Michang Granite and Its Dark Particle enclaves. *Acta Geosci. Sin.* **2011**, *32*, 293–303.

32. Anderson, P.L. Chemical composition of the mantle. *Geophys. Res.* **1983**, *88*, 41–52. [CrossRef]

33. Liu, Z.H.; Zhang, L.; Yang, C.X.; Wu, T.A.; Cui, X.F.; Ren, J.D.; Yang, C.Q. Magmatic mixing characteristics and significance of the Lushan rock mass in Lushan, Henan Province. *Geol. Surv. Res.* **2004**, *27*, 75–81.

34. Wang, Y.; Fan, W.; Peng, T.; Zhang, H.; Guo, F. Nature of the mesozoic lithospheric mantle and tectonic decoupling beneath the Dabie Orogen, central China: Evidence from 40Ar/39Ar geochronology, elemental and Sr-Nd-Pb isotopic compositions of early cretaceous mafic igneous rocks. *Chem. Geol.* **2005**, *220*, 165–189. [CrossRef]

35. Kocak, K. Hybridization of mafic microgranular enclaves: Mineral and whole-rock chemistry evidence from the Karamadaz Granitoid, Central Turkey. *Int. J. Earth Sci.* **2006**, *95*, 587–607. [CrossRef]

36. Zang, W.J.; Lai, S.C.; Qin, J.F.; Li, X.J.; Luo, J.C. Geochemistry and genesis of the dark-colored enclaves of the Wulong rock mass in the South Qinling Mountains. *J. Northwest Univ. Nat. Sci. Ed.* **2011**, *41*, 278–284.

37. Sun, S.S.; McDonough, W.F. Chemical and isotopic systematics of oceanic basalts: Implications for mantle composition and processes. *Geol. Soc.* **1989**, *42*, 313–345. [CrossRef]

38. Rudnick, R.L.; Gao, S. Composition of the Continental Crust. In *Treatise on Geochemistry*; Holland, H.D., Turekian, K.K., Eds.; Pergamon: Oxford, UK, 2003; pp. 1–64.

39. Chen, L.G.; Wang, B.Y.; Chen, L.R.; Zhang, B.; Dai, X.Y. Theenclaves characteristics and indication significance of granites in Huashan Mountain. *Shanxi Geol.* **2003**, *21*, 61–66.

40. Taylor, S.R.; McLennan, S.M. *The Continental Crust: Its Composition and Evolution*; Blackwell: Oxford, UK, 1985; 312p.

41. Wang, Y.W.; Wang, J.B.; Wang, S.L.; Wang, L.J.; Ding, R.F.; Pu, K.X. Magmatic mixing and its metallogenic significance in the Xiuli Kuduk area, Fuyun, Xinjiang. *J. Geol.* **2008**, *82*, 221–233.

42. Zhang, Y.M.; Zhang, H.F.; Liu, W.C.; Zhou, Z.G. Age and genesis of Damiao rock mass in Siziwangqi, central Inner Mongolia. *J. Petrol.* **2009**, *25*, 3165–3181.

43. Ahmad, M. Enclavess in granitoids of north of Jonnagiri schist belt, Kurnool district, Andhra Pradesh: Evidence of magma mixing and mingling. *J. Geol. Soc. India* **2011**, *77*, 557–573. [CrossRef]

44. Liu, L.; Qiu, J.S.; Li, Z.; Li, Y.L. The genesis of the Early Cretaceous quartz monzonite in Longyou, Zhejiang Province: The elements of the mafic enclaves and host rocks and the Sr-Nd isotope geochemical evidence. *J. Rock* **2012**, *28*, 3993–4006.

45. Rubatto, D.; Gebauer, D. Use of cathodoluminescence for U-Pb zircon dating by IOM Microprobe: Some examples from the western Alps. In *Cathodoluminescence Geosci.*; Springer: Berlin, Germany, 2000; pp. 373–400.

46. Wu, Y.B.; Zheng, Y.F. Zircon genesis mineralogy and its constraints on U-Pb age interpretation. *Sci. Bull.* **2004**, *49*, 1589–1604. [CrossRef]

47. Song, S.G.; Niu, Y.L.; Zhang, L.F.; Zhang, G.B. Time constraints on orogenesis from oceanic subduction to continental subduction, collision and exhumation: An example from North Qilian and North Qaidam HP-UHP belts. *Acta Petrol. Sin.* **2009**, *25*, 2067–2077.

48. Vernon, R.H. Microgranitoid enclaves in granites: Globules of hybrid magma quenched in a rock massic environment. *Nature* **1984**, *309*, 438–439. [CrossRef]

49. Dahlquist, J.A. Mafic microgranular enclaves: Early segregation from metaluminous magma (Sierra de Chepes), Pampean Ranges, NW Argentina. *J. S. Am. Earth Sci.* **2002**, *15*, 643–655. [CrossRef]

50. Donaire, T.; Pascual, E.; Pin, C. Microgranular enclaves as evidence of rapid cooling in granitoid rocks: The case of the Los Pedroches granodiorite, Iberian Massif, Spain. *Contrib. Mineral. Petrol.* **2005**, *149*, 247–265. [CrossRef]
51. Chappell, B.W. Magma mixing and the production of compositional variation within granite suites: Evidence from the granites of Southeastern Australia. *J. Petrol.* **1996**, *37*, 449–470. [CrossRef]
52. White, A.J.R.; Chappell, B.W.; Wyborn, D. Application of the restite model to the Deedick granodiorite and its enclaves: A reinterpretation of the observations and data of Maas et al. (1997). *J. Petrol.* **1999**, *40*, 413–421. [CrossRef]
53. Silva, M.V.G.; Neiva, A.M.R.; Whitehouse, M.J. Geochemistry of enclavess and host granites from the Nelas area, central Portugal. *Lithos* **2000**, *50*, 153–170. [CrossRef]
54. Fan, L.T.; Fang, S.Y.; Tao, Z.J.; Liang, Y.D. Discovery of Dark Microgranular enclaves (MME) in Uranium Granite of Miaoershan and Crust-Mantle Interaction. *J. Mineral.* **2009**, *29*, 625–626.
55. Xue, Y.S.; Liu, Z.J.; Wang, J.P.; Cheng, S.B. Characteristics of the Dark Particles of Granite and Its Research Direction. *Contrib. Geol. Miner. Resour. Res.* **2014**, *29*, 20–30.
56. Kim, J.S.; Shin, K.C.; Lee, J.D. Petrographical study on the Yucheon granite and its enclaves. *Geosci. J.* **2002**, *6*, 289–302. [CrossRef]
57. Vernon, R.H. Restite, xenoliths and microgranitoid enclavess in granites. *J. Proc. R. Soc. N. S. W.* **1983**, *116*, 77–103.
58. Piccoli, P.M.; Candela, P.A. Apatite in igneous system. *Rev. Mineral. Geochem.* **2002**, *48*, 255–292. [CrossRef]
59. Wyllie, P.J.; Cox, K.G.; Biggar, G.M. The habit of apatite in synthetic systems and igneous rocks. *J. Petrol.* **1962**, *3*, 238–242. [CrossRef]
60. Chappell, B.W.; White, A.J.R.; Wyhorn, D. The importance of residual source material (restite) in Granite Petrogenesis. *J. Petrol.* **1987**, *28*, 1111–1138. [CrossRef]
61. Liu, M.; Zhao, Z.D.; Guan, Q.; Dong, G.C.; Mo, X.X.; Liu, Y.S.; Hu, Z.C. The magma mixing genes of the Early Jurassic meta-granite and its enclaves in the Nierong micro-continent, Tibet: Zircon LA-ICP-MS U-Pb dating and Hf isotope evidence. *J. Rock* **2011**, *27*, 1931–1937.
62. Zang, W. Study on the Magmatic Mixing of the Late Triassic Wulong Rock Mass in the South Qinling Orogenic Belt. Ph.D. Thesis, Northwestern University, Xi'an, China, 2011.
63. Zhou, X.R. Granite mixing effect. *Front. Geosci.* **1994**, *1*, 87–97.
64. Zhou, L.F. Early Paleozoic tectonic features and evolution in the southern margin of the Alashan block. *J. Northwest Univ.* **1992**, *22*, 107–115.
65. Xia, L.Q.; Xia, Z.C.; Xu, X.Y. The genesis of volcanic magma in the Ordovician arc basin of the North Qilian Mountains. *China Geol.* **2003**, *30*, 48–60.
66. Zhou, T.Z.; Chen, J.F.; Zhang, W.; Li, X.M. Geochemical characteristics of the North Huaiyang granite-syenite belt and its tectonic significance. *Geol. Rev.* **1995**, *41*, 144–151.
67. Wang, X.X.; Wang, T.; Ilmari, H.; Lu, X.X. The magmatic mixing genesis and petrological significance of mafic enclaves in the Qinling ring-spotted granite: Elemental and Nd, Sr isotope geochemical evidence. *J. Rock* **2005**, *21*, 935–946.
68. Mo, X.X.; Luo, Z.H.; Deng, J.F.; Yu, X.H.; Liu, C.D.; Chen, H.W.; Yuan, W.M.; Liu, Y.H. East Kunlun orogenic belt granite and crustal growth. *J. Geol. Univ. China* **2007**, *13*, 403–414.
69. Mo, X.X. Magma effect and evolution of the Qinghai-Tibet Plateau. *Coll. Geol.* **2011**, *17*, 351–367.
70. Qin, J.F.; Lai, S.C.; Li, Y.F. Slab breakoff model for the triassicpost-collisional adakitic granitoids in the Qinling orogenic velt, central China: Zircon U-Pb ages, geochemistry and Sr-Nd-Pb isotopic constaints. *Int. Geol. Rev.* **2008**, *50*, 1080–1104. [CrossRef]
71. Deng, J.F.; Zhao, H.L.; Mo, X.X.; Wu, Z.X.; Luo, Z.H. *Root-Column Structure of the Chinese Mainland: The Key to Continental Dynamics*; Geological Publishing House: Beijing, China, 1996; pp. 14–82.
72. Jin, Z.M.; Gao, S. Bottom intrusion and its dynamic significance of crust-mantle evolution. *Geol. Sci. Inf.* **1996**, *15*, 1–7.
73. Huppert, H.E.; Sparks, R.S.J. The generation of granitic magmas by intrusion of basalt into continental crust. *J. Petrol.* **1988**, *29*, 599–624. [CrossRef]
74. Ma, C.Q.; Wang, R.J.; Qiu, J.Y. The origin of granitic magma and the sign of multiple magma mixing: Baoshangyi takes Beijing Zhoukoudian rock mass as an example. *Geol. Rev.* **1992**, *38*, 109–119.

75. Xu, Y.J.; Du, Y.S.; Cawood, P.; Guo, H.; Huang, H.; An, Z.H. Detrital zircon record of continental collision: Assembly of the Qilian Orogen, China. *Sediment. Geol.* **2010**, *230*, 35–45. [CrossRef]
76. Xia, L.Q.; Xia, Z.C.; Zhao, J.T.; Xu, X.Y.; Yang, H.Q.; Zhao, D.H. Determination of the properties of the Proterozoic continental overflow basalt in the western segment of the North Qilian Mountains. *Chin. Sci.* **2000**, *30*, 1–8.
77. Wu, F.Y.; Li, X.H.; Yang, J.H.; Zheng, Y.F. Several problems in the study of granite genesis. *J. Rock* **2007**, *23*, 1217–1238.